IEEE Access
Multidisciplinary ⋮ Rapid Review ⋮ Open Access Journal

Received July 10, 2021, accepted August 10, 2021, date of publication August 13, 2021, date of current version August 20, 2021.

Digital Object Identifier 10.1109/ACCESS.2021.3104619

Spectro-Temporal Combining in Bistate WiFi Backscatter Communication With Frequency Shift

HWANWOONG HWANG[1], RICHARD BOATENG NTI[2], AND JI-HOON YUN[2], (Member, IEEE)

[1]Department of Electrical and Information Engineering, Seoul National University of Science and Technology, Seoul 01811, South Korea
[2]Department of Electrical and Information Engineering and Research Center for Electrical and Information Technology, Seoul National University of Science and Technology, Seoul 01811, South Korea

Corresponding author: Ji-Hoon Yun (jhyun@seoultech.ac.kr)

This work was supported by the Basic Science Research Program through the National Research Foundation of Korea (NRF) through the Ministry of Education under Grant 2019R1A6A1A03032119 and Grant 2020R1F1A1077402.

ABSTRACT In WiFi backscatter communication, the frequency shift technique allows a backscattered signal to appear not in the frequency channel of the carrier signal but in adjacent ones, thus avoiding noisy OFDM-based carrier signals and increasing the communication range. Through testbed experiments, we observe that frequency shift is effective in mitigating the impact of the inherent fluctuation of WiFi signals, particularly in bistate backscatter communication; however, due to the weak strength of the backscattered signal, other signals from incumbent transmitters may appear in the shifted frequency channels, significantly interfering with the backscattered signal. To combat this challenge in a way that is nondisruptive to incumbent transmitters, we propose a receiver-side spectro-temporal combining scheme in which spectrum combining is performed to suppress interference appearing in one of the shifted channels, while temporal combining is performed with transmission repetitions to suppress bit errors resulting from residual interference. The scheme's on-the-fly spectrum combining and bit-sequence temporal combining require minimal buffer memory. Through system prototyping and testbed experiments, we demonstrate that the proposed scheme outperforms the conventional and temporal-combining-only cases in terms of the bit error rate and throughput under various conditions.

INDEX TERMS Ambient backscatter communication, WiFi backscatter, ultralow-power communication, frequency shift, interference suppression.

I. INTRODUCTION

Ambient backscatter communication [1] has recently received much attention for ultralow-power communication among low-end tag-type devices (e.g., sensor nodes) with the aid of existing signal sources in Internet of Things (IoT) environments. It is realized by allowing a tag device to reflect and absorb ambient signals in the air, such as TV broadcast signals [1], [2], FM radio signals [3], LoRa signals [4], Bluetooth signals [5], mmWave signals [6], or signals from multiple sources [7]–[9], in accordance with the data bits to be transmitted; thus, there is no need for the deployment of infrastructure for dedicated signal sources. Then, the amplitude, phase, or both of the carrier signal will be modulated accordingly so that a receiver can decode the data bits from it. By eliminating the need for the tag itself to perform carrier-signal generation and amplification, which are the most power-hungry tasks, ambient backscatter communication realizes ultralow-power operation. In particular, WiFi backscatter communication [10] has received considerable attention, mainly due to the wide availability of WiFi signal sources and WiFi-equipped user devices.

Bistate backscatter communication—in which a transmitter modulates the amplitude of a carrier signal into two levels (as a tag does by switching between the reflection and absorption states) and a receiver detects these levels by means of an amplitude threshold—provides a universal transmitter and receiver framework for all communication types, i.e., downlink (gateway-to-tag), uplink (tag-to-gateway), and tag-to-tag communication, thanks to its simplicity of implementation. Therefore, bistate amplitude modulation and threshold-based decoding are still of importance, even in WiFi backscatter communication. However, decoding data bits from bistate-backscattered WiFi signals is challenging since a WiFi signal itself has inherent fluctuations due to the high peak-to-average-power-ratio (PAPR) nature of orthogonal frequency-division multiplexing (OFDM). As the reflection gain of the tag decreases, the fluctuations of

The associate editor coordinating the review of this manuscript and approving it for publication was Eyuphan Bulut.

the WiFi carrier signal begin to overwhelm the amplitude patterns of the bistate-backscattered signal, resulting in a short communication range.

The *frequency shift* technique allows a backscattered signal to appear in other frequency channels, shifted from that of its carrier signal, thereby avoiding the influence of the WiFi signal fluctuation [11]. Thus, the receiver can obtain cleaner samples of the backscattered signal alone, and the communication range of WiFi backscatter communication is greatly enhanced. As will be illustrated by our experimental observations (Section III), the frequency shift technique is more powerful when combined with bistate amplitude modulation. A backscattered signal appears in a shifted frequency channel only when a tag reflects, not when it absorbs. Therefore, the difference in the signal samples between the reflection mode (a signal appears) and the absorption mode (noise floor) of a tag becomes more noticeable, making the threshold configuration straightforward and invariant in time.

However, in the field, the frequency shift technique is seriously limited by interference from incumbent transmitters in the shifted frequency channels, which is a challenge that thus far remains unexplored in the literature. Since the backscattered signal is generally too weak to be detected by other transmitters above a listen-before-talk (LBT) energy detection threshold and its carrier signal is not present in the shifted frequency channels, one or more signals interfering with the backscattered signal may appear, which will typically be much stronger than the backscattered signal itself, thus causing reception to fail. Considering a universal receiver framework including tags, the differentiation or cancellation of such interference would not be affordable for simple tag-level hardware and processing. Therefore, a means of making a frequency-shifted backscattered signal resilient against shifted-channel-incumbent transmission activities without disrupting those activities is crucial to allow the benefits of frequency shift to be fully exploited.

In this paper, we propose a new approach, named *spectro-temporal combining*, to combat the abovementioned interference problem arising in WiFi backscatter communication with frequency shift. The proposed approach can also be combined with a wide range of other solutions for further enhancement. First, we present experimental observations concerning how frequency shift mitigates the impact of the inherent fluctuation of WiFi signals, particularly in bistate backscatter communication, but suffers from signal interference from incumbent transmitters on the shifted frequency channels. We also observe that simple multiplicative combining of the backscattered signals received in upper and lower shifted frequency channels may suppress such interference, but the combined signal is vulnerable to interference appearing in both channels simultaneously. Therefore, to solve this interference problem, we design a scheme in which spectrum combining is performed to suppress interference appearing in one of the shifted frequency channels, while temporal combining is performed with transmission repetitions to suppress bit errors resulting from residual interference. This scheme is cost-efficient in terms of buffer memory consumption since spectrum combining is performed on the fly for incoming signals and temporal combining is performed between two bit sequences. Moreover, the scheme is a receiver-side solution and will not disrupt the activities of shifted-channel-incumbent transmitters.

The proposed scheme solves the shifted-channel-incumbent interference problem of the frequency shift technique—which has not previously been explored in the literature—in a cost-efficient way: (1) the tag hardware and software remain unchanged for tags equipped with frequency shift capabilities; (2) the receiver stores information bits, not signal samples, for combination with subsequently received information, thus operating at a low memory cost; and (3) the combining process of the scheme relies on only primitive multiplication and AND operations, thus having low processing power requirements.

Via a prototype implementation and testbed experiments, we demonstrate that the proposed scheme outperforms the conventional, temporal-combining-only, and code repetition cases in terms of the bit error rate and throughput under various communication conditions.

In summary, the main contributions of our work are listed as follows:

- Experimental observation and identification of the problem of shifted-frequency-incumbent interference encountered when the frequency shift technique is applied in WiFi backscatter communication.
- Design of a low-memory-cost scheme of spectro-temporal combining for interference suppression and reliable decoding in bistate WiFi backscatter communication with frequency shift.
- System prototyping and testbed experiments to validate the effectiveness of the proposed scheme in realistic communication environments.

The rest of the paper is organized as follows. In Section II, related works are reviewed. Section III presents important observations regarding the frequency shift technique based on testbed experiments. The proposed scheme is described in Section IV. The experimental setup and performance results are given in Section V. Finally, Section VI concludes the paper.

II. RELATED WORK

Many research works on backscatter communications have been conducted with diverse subjects [12]. Vougioukas and Bletsas [13] proposed both analog and digital tag modulation schemes based on switching frequency control at the tag. ReflectFX [14] reuses the received interfering carrier signals to transfer information such that the end user receives a self-interference-free signal. A cloud radio access network architecture was proposed in [15], in which the suppression of carrier signal interference for backscatter communication is managed by the cloud processor. A multiple-input multiple-output (MIMO) backscatter system was developed in [16], in which the diversity features of MIMO are leveraged

by implementing space-time coding on the tag. Backscatter communication over OFDM-modulated carrier signals has also been studied. Yang *et al.* [17] studied a joint design for the backscatter waveform and the receiver detector for ambient OFDM-modulated signals. ElMossallamy *et al.* [18] proposed a modulation scheme allowing both binary and higher-order modulation using noncoherent energy detection over ambient OFDM signals and analyzed its error performance. In [19], the noncoherent maximum-likelihood detection problem for a general Q-ary signal constellation was solved, and a suboptimal detector was derived. There have also been attempts to analyze the performance of backscatter communication. In [20], the performance of wireless broadband networks with ambient backscatter tags was analyzed considering the interference arising from the backscatter tags. The performance of an underlay spectrum sharing backscatter communication system was analyzed in [21].

WiFi has also been considered a strong candidate for ambient signal sources, and some recent works have studied backscatter communication on this basis. The initial attempt was made in [10] by considering a conventional backscatter tag and threshold-based bit decoding from the per-frame received signal strength or channel state information. BackFi [22] improved the data rate by using a full-duplex radio at the receiver side as a signal source and a receiver simultaneously to decode backscattered signals against the self-interference of WiFi signals, but at the expense of increased complexity. TScatter [23] is an OFDM backscatter system that uses high-granularity sample-level modulation to avoid the phase offset created by a tag being eliminated by phase error correction. Renjie *et al.* [24] developed orthogonal frequency-division multiple access (OFDMA) in WiFi backscatter, where OFDMA is realized by coordinating backscatter tags to concurrently convey information to the receiver with orthogonal subcarriers. SyncScatter [25] enables symbol-level synchronization through a hierarchical wakeup and synchronization protocol. WiTAG [26] sends data by selectively interfering with subframes in an aggregated WiFi frame, enabling standard-compliant communication. MOXcatter [27] works with multiple spatial streams of ambient WiFi signals. X-Tandem [28] is a multihop backscatter system in which tags work as relays for each other and their data are modulated into a single backscatter packet. GuardRider [29] uses Reed-Solomon codes for forward error correction and adjusts backscatter transmission following statistical knowledge of WiFi traffic. WiFi backscatter and radio frequency identification (RFID) technologies were compared in [30] in terms of RF harvesting capabilities, throughput, range and scalability.

There have also been later attempts to enhance the performance of WiFi backscatter communication when faced with the fluctuation of WiFi carrier signals. FS-Backscatter [11] adopts the frequency shift technique and greatly enhances the communication range by avoiding strong interference from the WiFi carrier signal at the receiver side. HitchHike [31] and FreeRider [32] enable commodity WiFi receivers to decode backscattered signals by allowing a tag to perform codeword translation of a received WiFi signal in order to convey data bits on that signal. These solutions require two receivers to capture signals in both the carrier and shifted frequency channels as well as another entity to combine these signals to finally decode the data bits. The authors of [33] proposed a pattern-matching-based decoding algorithm that identifies the unique patterns of signal samples that result from the smoothing of WiFi signals to filter out noisy fluctuations. In [34], the approach of combining repeated signals was shown to be effective in mitigating the fluctuation of WiFi carrier signals, and a repetition adaptation algorithm was designed. Decoding data bits from backscattered signals in unused subbands of a WiFi signal was proposed in [35]. A scheme consisting of channel-independent packet detection and error vector demodulation to decode a backscattered signal carried by a WiFi signal on a receiver's listening channel as well as adjacent channels was proposed in [36]. A multifilter design to exclude undesired interference from WiFi carrier signals was proposed in [37] for the effective decoding of WiFi backscattered signals.

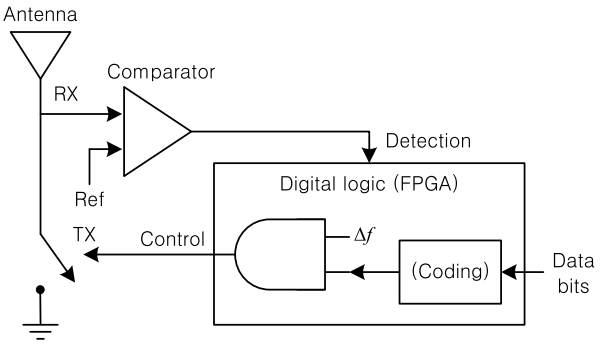

FIGURE 1. Block diagram of a WiFi-backscattering tag device with frequency shift capabilities.

While some prior research works have adopted the frequency shift technique to avoid the problem of WiFi carrier-signal fluctuation, the shifted-channel-incumbent interference problem of this technique has not yet been explored in the literature. The proposed approach, which is the first to tackle this problem, can also be combined with many of the aforementioned solutions for further enhancement.

III. EXPERIMENTAL OBSERVATIONS CONCERNING FREQUENCY SHIFT IN WIFI BACKSCATTER COMMUNICATION

A. IMPLEMENTATION OF FREQUENCY SHIFT

Fig. 1 shows a block diagram of our prototype tag design with frequency shift capabilities. The device consists of a detector for WiFi carrier signals and a transmitter. When a WiFi signal appears that has a received signal strength higher than a certain reference level, the transmission procedure of the digital logic (field-programmable gate array, FPGA) is triggered. The data bits to be transmitted optionally pass through a coding block (e.g., FM0) and are input into an

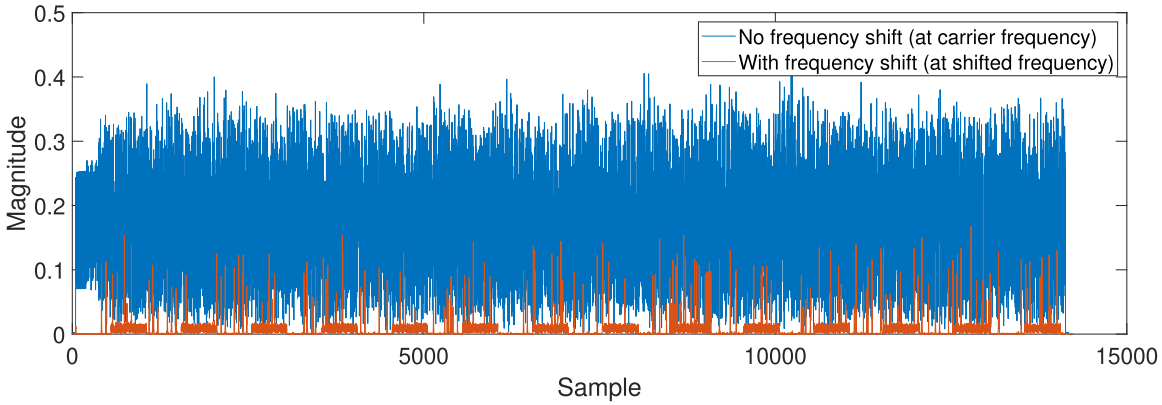

FIGURE 2. Backscattered signal samples with and without a frequency shift.

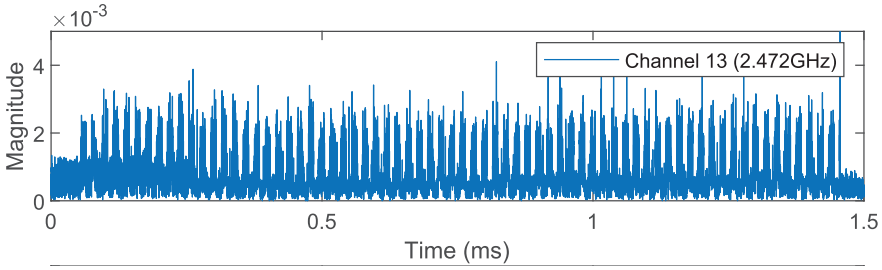

(a) Received signal in channel 13 (with no interference)

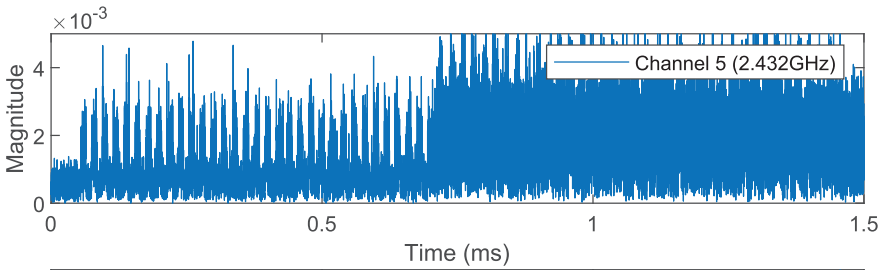

(b) Received signal in channel 5 (with interference)

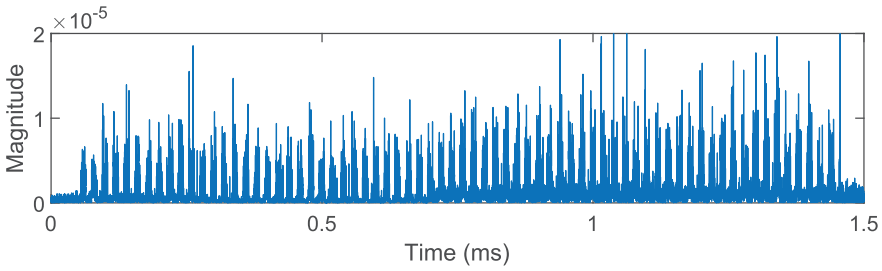

(c) Combined signal

FIGURE 3. Received signals in shifted frequency channels and the corresponding combined signal.

AND gate with a clock signal at a frequency of Δf, which is the amount by which the frequency is to be shifted from the carrier signal's frequency. The output signal of the AND gate is then input into the control port of an RF switch placed between the antenna and ground to control its state between reflection and absorption, corresponding to bit values of one and zero, respectively.

As a result, when the tag transmits a one bit, it alternates between reflection and absorption at Δf; thus, the backscattered signal appears at the carrier signal's frequency$\pm\Delta f$. When it transmits a zero bit, it remains in the absorption state, not backscattering the carrier signal.

B. EXPERIMENTS AND OBSERVATIONS

Backscattered-signal samples of alternating one and zero bits without and with a frequency shift for one WiFi data frame are illustrated in Fig. 2. The frequency of the WiFi signal is 2.452 GHz, and the magnitude of the frequency shift (Δf)

is set to 20 MHz; thus, the backscattered signal appears at 2.432 and 2.472 GHz. In the signal samples without a frequency shift (blue), the backscatter pattern is not observable due to the high fluctuation of the WiFi carrier signal. When the frequency shift technique is applied, the backscattered signal (orange) appears in shifted frequency channels when in the tag is in the reflection state and does not appear when it is in the absorption state. Therefore, a bistate backscatter pattern is clearly apparent and, thus, stably decodable.

One point to be noted is that with a frequency shift, differentiating the level of a backscattered signal's amplitude based on a threshold becomes more straightforward. This is because when the tag is in the absorption state, no backscattered signal appears in the shifted frequency channels, and the received energy level is near the noise floor. Therefore, the threshold for differentiating the signal amplitude levels can be simply set to $\alpha\times$ (noise floor), where $\alpha(>1)$ is a fixed coefficient corresponding to some margin, thus making the tricky threshold configuration procedure obsolete (we describe the details of the threshold configuration procedure in the next section).

However, interference from incumbent transmitters (e.g., WiFi access points (APs) and devices) in the shifted frequency channels may cause the decoding of the backscattered signal to fail. While Fig. 3(a)[1] shows a clear backscatter pattern without any interference in one shifted frequency channel, as in Fig. 2, Fig. 3(b) shows the received signal samples in the other shifted frequency channel, where an interfering transmission starts in the middle of the backscattered signal, causing a sudden change in the signal amplitude. If the threshold for differentiating amplitude levels is set equal to the noise floor level with some margin, the part of the signal that is affected by this interference will all be decoded as one due to the elevated amplitude. Making the threshold track such sudden amplitude changes in real time is challenging and is likely to result in decoding errors at the beginning of interference and even during interference due to the aforementioned fluctuating nature of the interfering WiFi signal.

Fig. 3(c) shows the signal resulting from multiplicative combining of the two signals in Fig. 3(a) and (b). After the signals are combined, the amplitude of the zero bits is significantly decreased to close to the noise floor, while that of the one bits is still high. This interference suppression effect originates from the fact that the signal amplitude is near the noise floor when the tag is in the absorption state. Such signal combining is also effective in the part of the signal without interference, significantly increasing the signal amplitude of the one bits while maintaining that of the zero bits close to the noise floor. However, the interference suppression effect is obtained only when the interference appears in only one shifted frequency channel at a time. If interference appears in both of the shifted frequency channels simultaneously, which is possible due to wideband transmission devices[2] or simple coincidence, spectrum combining alone cannot completely suppress such interference.

[1]The experimental setup in Fig. 3 is slightly different from that in Fig. 2. In Fig. 3, the tag's bit rate is 100 kbps, and the received signals undergo moving-average filtering to reduce the fluctuation of the WiFi signal.

IV. SPECTRO-TEMPORAL COMBINING SCHEME

Fig. 4 illustrates the processing flow of the proposed scheme. In what follows, we describe the details of the scheme and explain the rationale behind the design.

A. SPECTRUM COMBINING

It is assumed that a backscatter tag is equipped with frequency shift capabilities and backscatters WiFi carrier signals into upper and lower adjacent frequency channels, which we denote by f_1 and f_2, respectively. A receiver listens to both channels and extracts the backscattered signals individually. The received signals may first be passed through individual low-pass filters to alleviate the remaining fluctuation of the WiFi carrier signal. Then, the receiver performs either multiplication or summing of the two signals, which corresponds to *spectrum combining*. Subsequently, the combined signal enters a decoding block, in which the signal amplitude levels are differentiated by means of a threshold into one or zero bits. The proposed spectrum combining process is performed on the fly on the incoming streams of received signals, with no buffering of the signal samples, which is important to ensure that the complexity and cost of the receiver are affordable.

In the following, we further detail how the proposed spectrum combining procedure suppresses interference. Let $y_i(t)$ be the tth received signal sample at frequency f_i ($i \in \{1, 2\}$), and let $c(t)$ be the WiFi carrier signal. We denote the information signal of the tag, i.e., the data bit (one or zero) transmitted by the tag, by $x(t)$ ($\in \{0, 1\}$). If a one (zero) bit corresponds to the tag's reflection (absorption) state, the received signal $y_i(t)$ is obtained as follows:

$$y_i(t) = h_i(t)x(t)c(t) + I_i(t) + \sigma, \tag{1}$$

where $h_i(t)$ is the channel gain of the backscatter path from the WiFi carrier source to the receiver through the tag, $I_i(t)$ is the interference signal at f_i and σ is the noise floor.[3] Spectrum combining of the two received signals $y_1(t)$ and $y_2(t)$ produces a combined signal by multiplication, denoted by $y_{sc}(t)$ and obtained as $y_1(t) \times y_2(t)$. Then, a threshold of $\alpha \cdot \sigma$ is applied to $y_{sc}(t)$ to differentiate its amplitude into two levels, which correspond to the bit values. Here, the coefficient $\alpha(>1)$ is configured as described below.

Proposition 1: If the threshold $\alpha \cdot \sigma$ for differentiating the amplitude of a spectrum-combined signal into two levels corresponding to one and zero bits is configured based on the condition of no interference, it satisfies

$$\sigma^2 < \alpha \cdot \sigma < \Pi_i(h_i(t)c(t) + \sigma).$$

[2]IEEE 802.11ac/ax allows transmission over up to 160 MHz, which corresponds to 8 nonoverlapping frequency channels.

[3]We assume that the fluctuation of the noise floor is much smaller than that of the other signals (as seen in Figs. 2 and 3) and thus negligible.

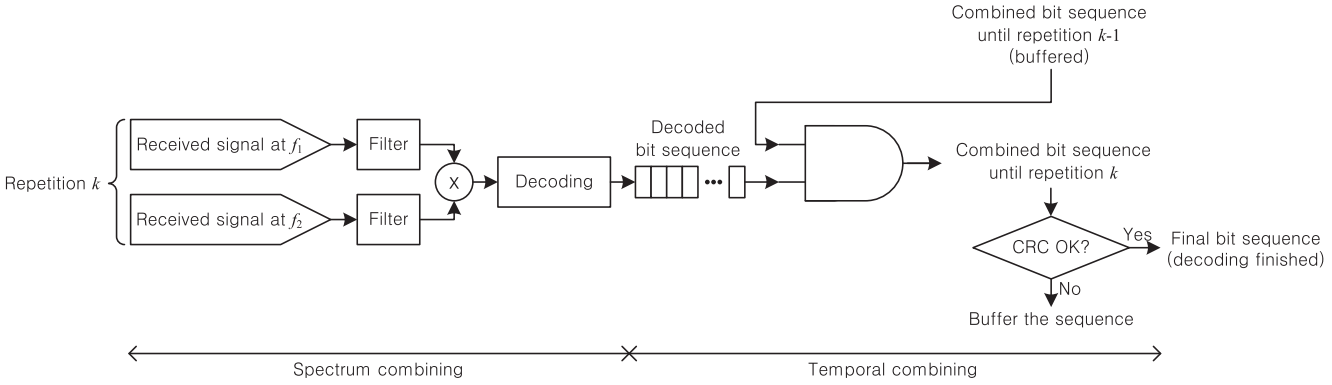

FIGURE 4. Processing flow of the proposed spectro-temporal combining scheme.

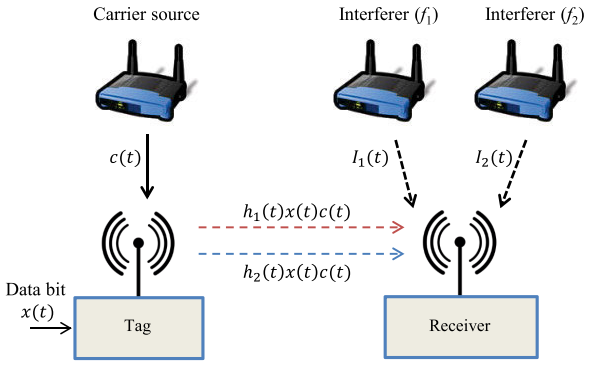

FIGURE 5. System model.

Proof: After multiplicative combination of the two signals received from the shifted frequency channels, with no interference, the combined signal $y_{sc}(t)$ is obtained as $(h_1(t)c(t) + \sigma)(h_2(t)c(t) + \sigma)$ for $x(t) = 1$ and as σ^2 for $x(t) = 0$. Thus, the threshold can be configured between these two values. ■

Proposition 2: Suppose that there exists a constant $\hat{\alpha}$ that satisfies the following condition for all t:

$$\sigma^2 < \hat{\alpha} \cdot \sigma < \min_t \Pi_i(h_i(t)c(t) + \sigma).$$

Then, the required range of α to configure a time-invariant threshold is given as

$$\sigma < \alpha \leq \hat{\alpha}.$$

Proof: The proof is straightforward, so we omit the details. ■

When a threshold configured in accordance with the combined signal is applied, the decoding result depends on the transmitted bit value and the presence of interference, as described below:

- When $x(t) = 1$ (one bit): We always have $y_{sc} > \alpha \cdot \sigma$ regardless of $I_i(t)$. Therefore, no decoding error occurs.
- When $x(t) = 0$ (zero bit): The decoding result depends on the presence of interference in each channel.
  - $I_i(t) = 0, \forall i$: $y_{sc} = \sigma^2$, which satisfies $y_{sc} < \alpha \cdot \sigma$, thus resulting in decoding success.
  - $I_1(t) > 0$ and $I_2(t) = 0$ or $I_1(t) = 0$ and $I_2(t) > 0$: We obtain $y_{sc}(t) = \sum_i I_i(t) \times \sigma$. If α is configured in accordance with Proposition 1 and $I_i(t) \times \sigma < \Pi_i(h_i c + \sigma)$, no decoding error will occur.[4]
  - $I_i(t) > 0, \forall i$: In this case, $y_{sc}(t)$ contains the term $I_1(t) \times I_2(t)$, which, in general, is much greater than $\Pi_i(h_i c + \sigma)$ and thus greater than the threshold. Therefore, decoding error always occurs.

As described above, spectrum combining can suppress the effect of interference when it is present in only one of the shifted frequency channels but cannot do so if interference is present in both channels simultaneously. Such situations are therefore handled through temporal combining, as described in the next subsection.

Additive combination of the two signals received from the shifted frequency channels can also be performed to obtain a combined signal $y_{sc}(t)$. However, multiplicative combination is more beneficial in terms of the ratio of the signal levels for the two bit states, as shown in the following.

Proposition 3: Multiplicative combination of the two signals received from the shifted frequency channels for decoding results in a higher ratio of the signal amplitude for a one bit to that for a zero bit than additive combination does.

Proof: For multiplicative combination of the two signals, we obtain a combined signal with the form $(h1(t)c(t) + \sigma)(h2(t)c(t) + \sigma)$ for a one bit and σ^2 for a zero bit. Thus, the ratio between the signal amplitudes is $\frac{(h_1(t)c(t)+\sigma)(h_2(t)c(t)+\sigma)}{\sigma^2} = \frac{h_1(t)h_2(t)c^2(t)+(h_1(t)+h_2(t))c(t)\sigma}{\sigma^2} + 1$. For additive combination, this ratio has the form $\frac{(h_1(t)+h_2(t))c(t)+2\sigma}{2\sigma} = \frac{(h_1(t)+h_2(t))c(t)\sigma/2}{\sigma^2} + 1$. Therefore, multiplicative combination results in a greater ratio between the two signal states. ■

B. TEMPORAL COMBINING

Fig. 6 shows two spectrum-combined signals obtained for different WiFi frame signals; the transmitted bits are alternating ones and zeros at 100 kbps, and the decoded bits obtained from each signal are overlaid as red lines. Both

[4]Throughout our experiments, this condition was always met (since the noise floor (σ) was much lower than any other signals).

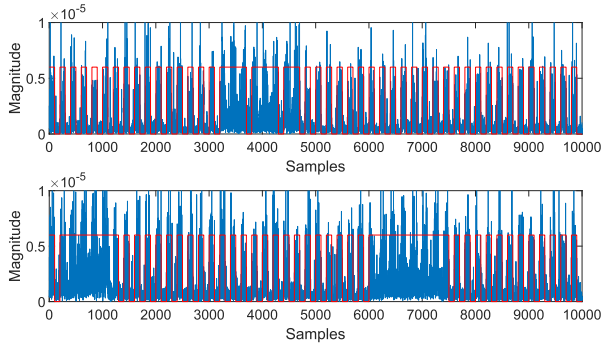

FIGURE 6. Received signals after spectrum combining (blue) for different WiFi frames and the decoded bits (red) for each.

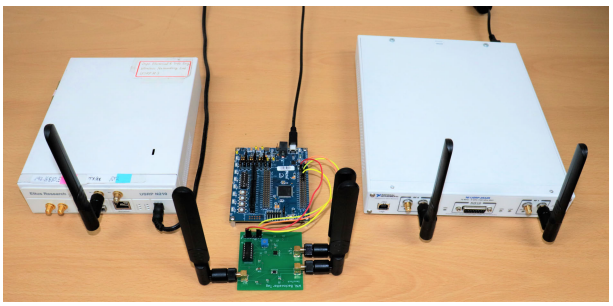

FIGURE 7. Tag hardware prototype and testbed configuration.

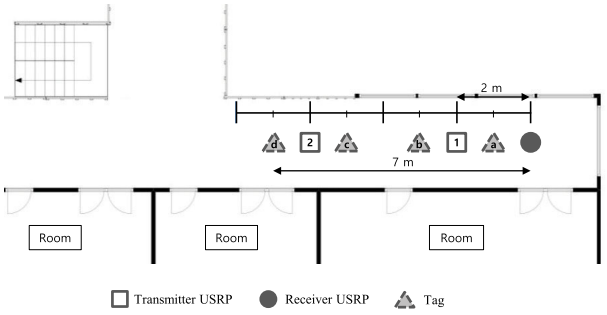

FIGURE 8. Experimental setup and tag positions.

signals suffer from some bit errors in which transmitted zero bits are decoded as one bits due to signal amplitude levels above the decoding threshold. Such bit errors that remain after spectrum combining, as mentioned before, result mostly from interference appearing simultaneously in both shifted frequency channels, which is consequently not suppressed by spectrum combining. Fortunately, the two signals in this figure do not undergo rises in their amplitude levels at the same position. If the two signals carry the same packet, we may be able to selectively take nonerroneous bits from both of them to obtain a complete packet with fewer or no bit errors. In general, it is unlikely for bit errors after spectrum combining to occur in the same position in distinct backscattered signals since the carrier source and other-channel transmitters behave independently.[5]

[5]If a WiFi carrier source performs a wideband transmission spanning the shifted frequency channels, backscattering with a frequency shift becomes equivalent to the case without a frequency shift, i.e., in-band backscattering.

Based on this idea, the proposed scheme adopts multiple transmission repetitions and the combination of the repeated signals, which we call *temporal combining*. The temporal combining procedure used in the proposed scheme is bit-level combining, i.e., an AND operation between the accumulated bit sequence and the new bit sequence. As illustrated in Fig. 4, the decoded bit sequence after spectrum combining is subjected to a bitwise AND operation with the accumulated bit sequence, which is the temporally combined result of the previous repetitions. Then, unless a bit error is present in the same bit position in two sequences, the bit errors in one sequence that appear as one bits are AND-ed with the error-free zero bits in the other sequence and corrected to zero bits in the output sequence. After the AND operation, the cyclic redundancy check (CRC) code of the output bit sequence is checked. If no bit errors are found, the final bit sequence is confirmed, and decoding is finished. If bit errors still exist, then the output bit sequence is stored as a new accumulated bit sequence for the next round of temporal combining.

Notably, the combining procedure of [34] is signal-level combining, which requires an extremely large buffer to store previous signal samples, while the proposed procedure requires only a packet-size buffer. In fact, the purpose of temporal combining differs between this work and [34]. We use temporal combining to eliminate bit errors that result from residual interference after spectrum combining and appear in random positions over transmission repetitions, while [34] focuses on mitigating the fluctuation of WiFi carrier signals by summing random fluctuation patterns out. Our scheme does not need temporal combining for fluctuation mitigation since this problem does not arise thanks to the adoption of the frequency shift technique and the time-invariant threshold configuration.

V. PERFORMANCE EVALUATION

In this section, we evaluate the proposed scheme via testbed experiments.

A. EXPERIMENTAL SETUP

Fig. 7 shows our tag hardware prototype and testbed configuration. The experimental setup is shown in Fig. 8.[6] We used two Ettus Universal Software Radio Peripherals (USRPs) (N210 and X310) [38]; one (N210) generated WiFi signals as a carrier source, and the other (X310) received backscattered signals as a backscatter receiver. The position of the receiver USRP (circle) was fixed, and the transmitter USRP (rectangle) was located either 2 or 6 meters away from the receiver, indexed as Positions 1 and 2, respectively, in Fig. 8. The backscatter tag (triangle) was first placed 1 meter away from the receiver and moved towards the transmitter USRP in increments of two meters until the tag was 7 meters away from the receiver; the corresponding tag positions are indexed

[6]The location is in a six-story building with ambient interference signals due to uncontrollable transmission activities of already-deployed WiFi access points and devices.

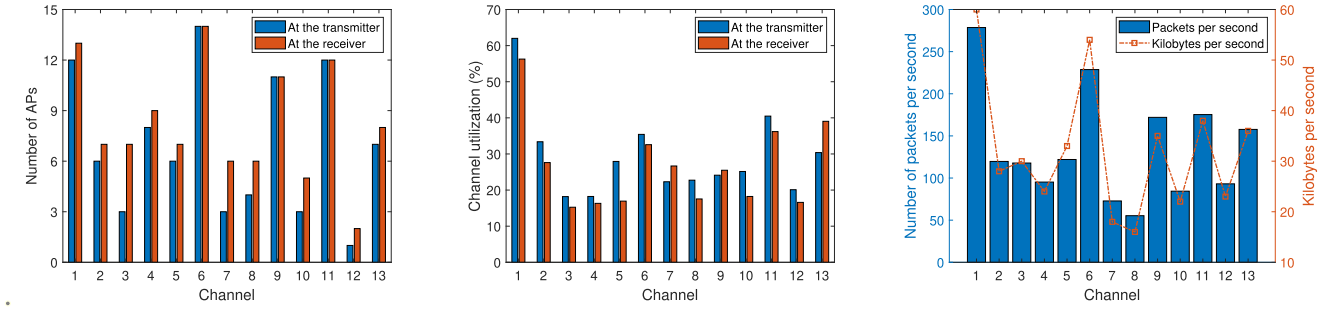

(a) Deployed APs (b) Channel utilization (c) Packets and traffic amount

FIGURE 9. Site survey results at the transmitter and receiver USRP positions.

as a, b, c, and d, respectively, in the figure. All nodes were placed 0.5 meters above the ground.

To generate WiFi carrier signals, the gr-ieee802-11 module of GNU Radio [39] was used, and IEEE 802.11g OFDM frames were generated. Each WiFi frame consisted of a 64 μs physical-layer header and a subsequent medium access control (MAC) frame of 1528 bytes. The transmitter USRP transmitted a WiFi frame every 10 ms, each with a time duration of 1.4 ms and a bit rate of 9 Mbps (with quadrature phase shift keying (QPSK) modulation and a 3/4 code rate). The transmitter USRP generated signals at center frequencies of 2.452 GHz (Channel 9) and 2.442 GHz (Channel 7). The receiver USRP captured the in-phase/quadrature (I/Q) signals of the received WiFi frames at two frequencies, 2.432 and 2.472 GHz (Channels 5 and 13) for the center frequency of 2.452 GHz (Channel 9) and 2.422 and 2.462 GHz (Channels 3 and 11) for the center frequency of 2.442 GHz (Channel 7), each at a sampling rate of 10 MHz. Then, each captured signal stream was smoothed via a moving average with a window size equal to the symbol length and was input into the decoding block. The value of α for threshold configuration was set to 1.2.[7] The backscatter tag was implemented using Analog Devices' RF switch ADG902 [40], connected to Microsemi's AGLN250 FPGA board [41] for control-signal generation. The tag transmitted data bits of alternating ones and zeros at a bit rate of 100 or 500 kbps. The magnitude of the frequency shift (Δf) was set to 20 MHz. In each experiment, the total number of generated WiFi frames was 500. The bit error rate (BER) and the throughput of data bits were considered as the performance metrics.

B. EVALUATION RESULTS

The BER performance of the proposed scheme is shown in Figs. 10 and 11 and compared with that of temporal combining alone for various tag-to-receiver distances (1, 3, 5, and 7 meters) and numbers of transmission repetitions (0, 1, 2, and 3) at two bit rates, for the carrier frequency of Channel 9. When the receiver does not detect backscattered signals at all, we set the BER to 0.5. In the figures, temporal combining with zero transmission repetitions and code repetition with code length one corresponds to the conventional approach with no combining. In Fig. 10, the tag is initially placed at the midpoint between the transmitter and receiver (1 meter distance) and becomes farther from both as the tag-to-receiver distance increases. At a distance of 7 meters, the tag is too far from both the transmitter and receiver and thus suffers disconnection. This figure shows that temporal combining alone also improves the BER, with an increase in gain with more transmission repetitions. Code repetition, in which every information bit is repeated a number of times equal to the code length during transmission and is decoded based on voting, also shows performance improvement as the code length increases, but the gain is limited compared with the other two schemes. When the proposed spectro-temporal combining scheme is applied, the BER performance is significantly improved over that of temporal combining alone in all cases except at a distance of 7 meters, which implies that interference suppression is effective in decreasing the BER. When the tag's bit rate is increased to 500 kbps, the BER increases in most cases. We observe similar trends in Fig. 11 when the transmitter is placed 6 meters away from the receiver, except for the case of a 7 meter distance, since the tag is farthest from the transmitter in this case. The BER reduction gain of the proposed scheme ranges from 43% (one repetition at 7 meters in Fig. 11(d)) to 95% (three repetitions at 1 meter in Fig. 10(c)). The BER results for the carrier frequency of Channel 7, which are presented in Figs. 12 (Position 1) and 13 (Position 2), show similar trends to those observed and discussed above. Thus, the proposed scheme is demonstrated to outperform temporal combining for various channel assignments. As shown in the site survey in Fig. 9, Channel 11 is more crowded than Channel 13, and thus, a signal that is frequency shifted to Channel 11 may experience interference more frequently when Channel 7 is the carrier than when Channel 9 is the carrier. Moreover, when Channel 7 is the carrier, there exist more interference sources in the upper channels of Channel 11 while Channel 13 receives interference from lower channels only. Therefore, the overall performance shown in Figs. 12 and 13 is lower than that in Figs. 10 and 11, respectively.

The throughput results are given in Fig. 14 and show even larger performance gaps between temporal combining alone

[7]For threshold configuration, the noise floor was measured as an average of signal samples with no tag transmission or interference in a captured signal trace.

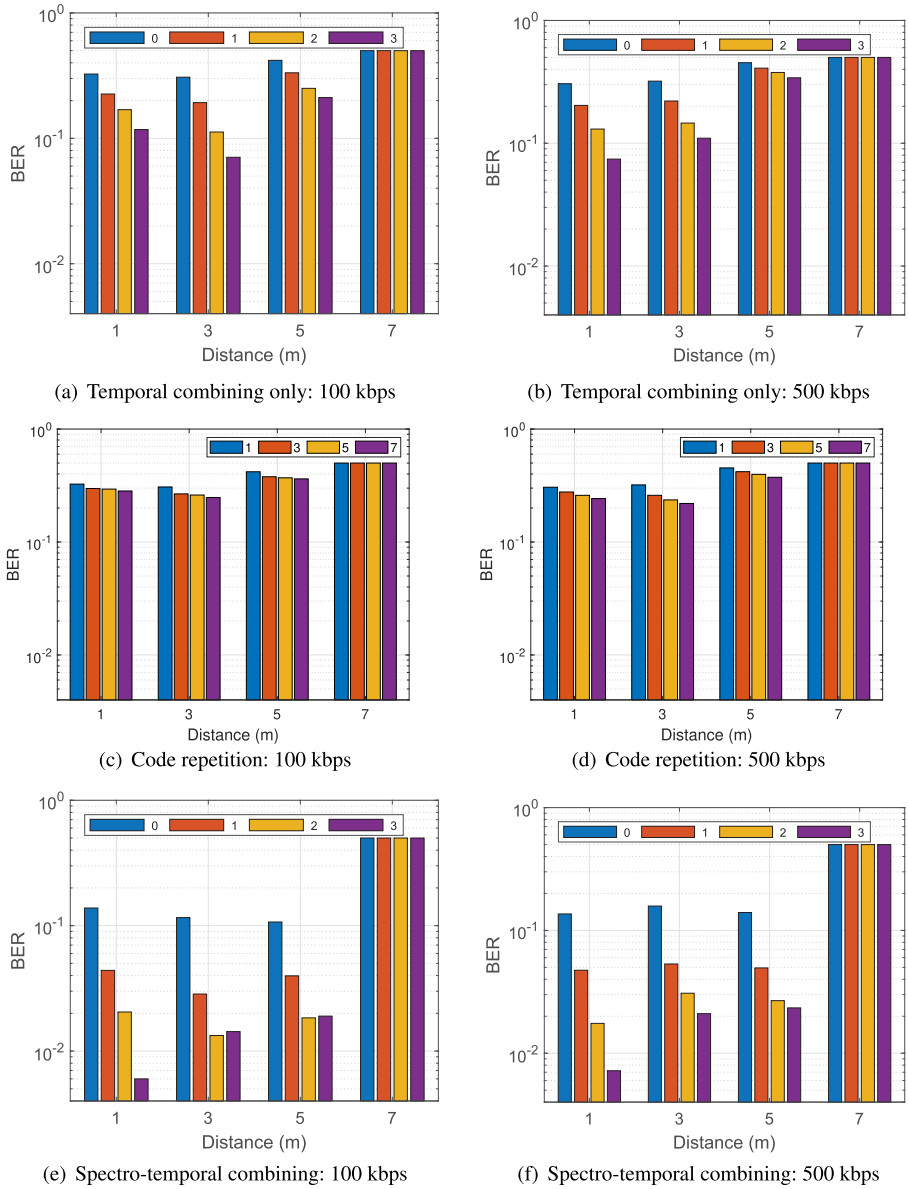

(a) Temporal combining only: 100 kbps

(b) Temporal combining only: 500 kbps

(c) Code repetition: 100 kbps

(d) Code repetition: 500 kbps

(e) Spectro-temporal combining: 100 kbps

(f) Spectro-temporal combining: 500 kbps

FIGURE 10. BER results when the carrier source (transmitter USRP) is in Position 1 (the transmitter-to-receiver distance is 2 meters) using Channel 9 for various tag-to-receiver distances and numbers of transmission repetitions.

and the proposed scheme. It is assumed that the tag transmits 50-bit packets back to back at a bit rate of 500 kbps during the first 1 ms of each WiFi frame, thus transmitting ten packets per WiFi frame. Since a WiFi frame is transmitted every 10 ms, the maximum achievable throughput (when zero BER is achieved with no transmission repetition) is 50 kbps. This figure shows that temporal combining alone is not a viable solution in the considered environment, resulting in zero or near-zero throughput in most cases. The proposed scheme with a sufficient number of transmission repetitions achieves significantly higher throughput than temporal combining. In some cases (5 meters in Position 1 and 3 meters in Position 2), two repetitions are slightly better than three repetitions, which implies that adaptation of the number of transmission repetitions as in [34] may still be beneficial to achieve the optimal throughput performance.

Fig. 15 shows the cumulative distribution functions (CDFs) of the per-frame BER, which is measured as the ratio of the number of erroneous bits to the total number of backscattered (transmitted) bits in a WiFi frame,[8] when the transmitter-to-receiver distance is two meters and the tag is placed at the midpoint between them. As seen from the CDF results, the transmission performance decreases as the bit rate of the backscatter tag increases. As also seen from the previous results, the proposed scheme significantly

[8]If we assume that one packet is transmitted per WiFi frame, a per-frame BER of zero corresponds to successful packet reception.

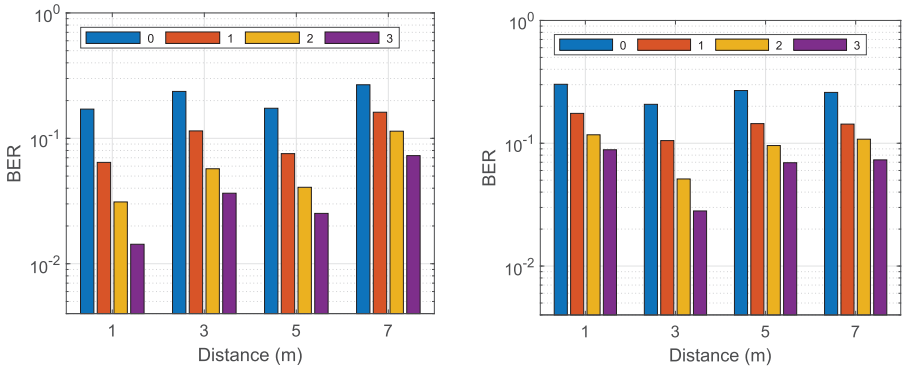

(a) Temporal combining only: 100 kbps (b) Temporal combining only: 500 kbps

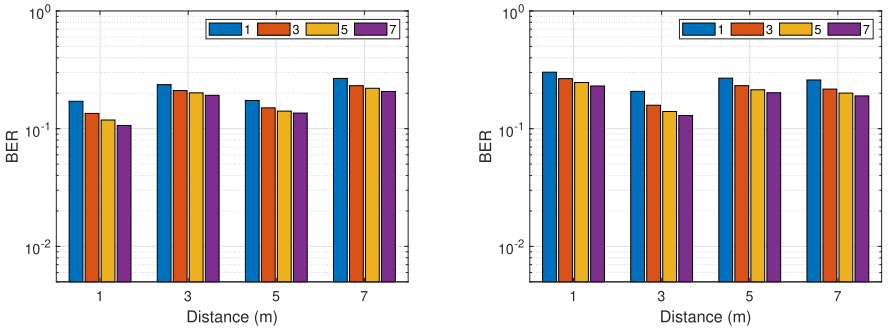

(c) Code repetition: 100 kbps (d) Code repetition: 500 kbps

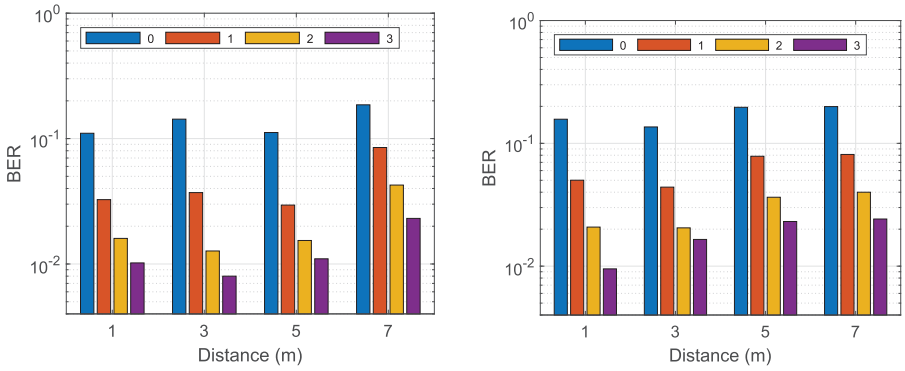

(e) Spectro-temporal combining: 100 kbps (f) Spectro-temporal combining: 500 kbps

FIGURE 11. BER results when the carrier source (transmitter USRP) is in Position 2 (the transmitter-to-receiver distance is 6 meters) using Channel 9 for various tag-to-receiver distances and numbers of transmission repetitions.

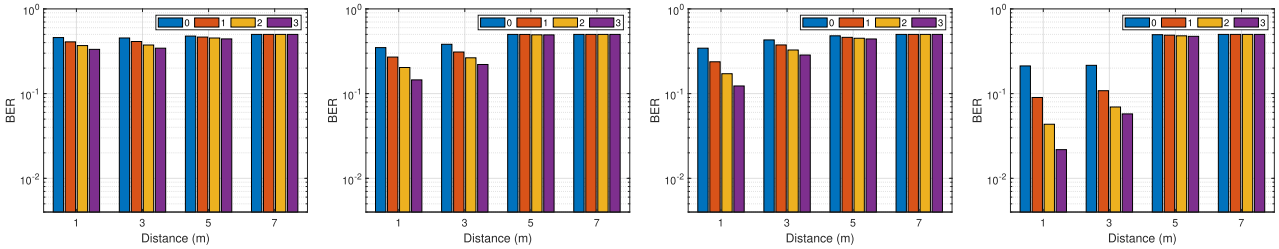

(a) Temporal combining: 100 kbps (b) Temporal combining: 500 kbps (c) Spectro-temporal combining: 100 kbps (d) Spectro-temporal combining: 500 kbps

FIGURE 12. BER results when the carrier source (transmitter USRP) is in Position 1 (the transmitter-to-receiver distance is 2 meters) using Channel 7 for various tag-to-receiver distances and numbers of transmission repetitions.

outperforms temporal combining alone, enabling a tag to achieve error-free transmission with three transmission repetitions for more than 80% of the WiFi frames at 100 kbps and 50% of them at 500 kbps, while temporal combining alone achieves error-free transmission for only approximately 40% and 20% of the WiFi frames, respectively.

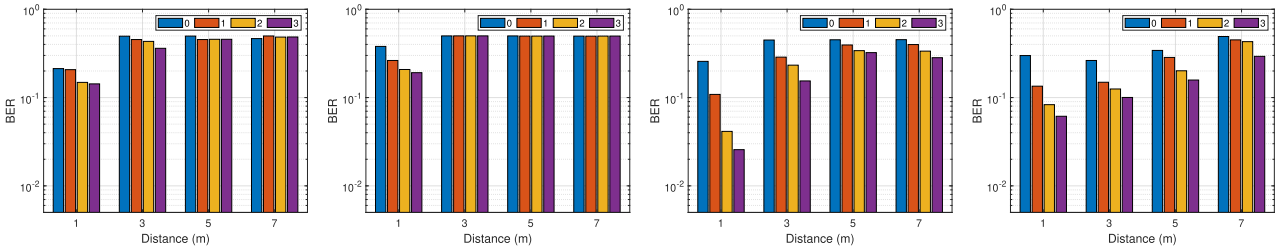

(a) Temporal combining: 100 kbps (b) Temporal combining: 500 kbps (c) Spectro-temporal combining: centering 100 kbps (d) Spectro-temporal combining: 500 kbps

FIGURE 13. BER results when the carrier source (transmitter USRP) is in Position 2 (the transmitter-to-receiver distance is 6 meters) using Channel 7 for various tag-to-receiver distances and numbers of transmission repetitions.

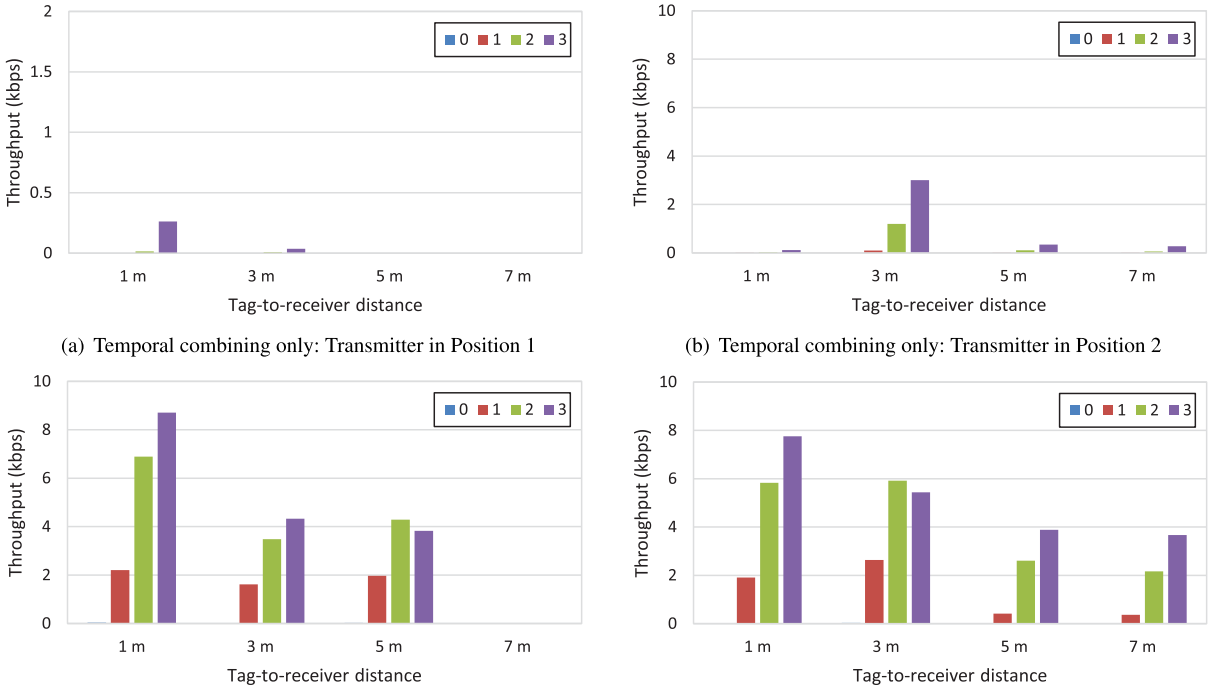

(a) Temporal combining only: Transmitter in Position 1 (b) Temporal combining only: Transmitter in Position 2

(c) Spectro-temporal combining: Transmitter in Position 1 (d) Spectro-temporal combining: Transmitter in Position 2

FIGURE 14. Throughput results for various tag-to-receiver distances and numbers of transmission repetitions (the tag's bit rate is 500 kbps, and the carrier frequency is Channel 9).

Performance degradation is generally observed when the bit rate is increased to 500 kbps.

To investigate the impact of the WiFi interference pattern on the performance in a controlled environment, we emulated interference signals on top of a signal trace recorded with the transmitter at Position 1 and the tag placed at the midpoint between the transmitter and receiver. We modeled the activity of the emulated WiFi signal source as a two-state Markov chain in which a signal is generated in the active state and is not generated in the idle state. We considered individual sources in both frequency-shifted channels. We assumed that the received signal level of the emulated WiFi source exceeded the level of the frequency-shifted signals, thus resulting in a decoding result of one bit in the corresponding channel. We set the mean length of an interference signal to $1/p_{ai}$, where p_{ai} is the probability of transitioning from the active state to the idle state in the Markov chain (we denote the probability of transitioning from the idle state to the active state by p_{ia}). Then, we varied the probability of interference being present in each channel, which is denoted by p and obtained as $p = p_{ia}/(p_{ia} + p_{ai})$. When an interference signal appeared in one frequency-shifted channel, we allowed an interference signal to appear simultaneously in the other frequency-shifted channel with a probability of 0.1 to mimic wide-bandwidth signals. The BER results are shown in Fig. 16. When the mean interference length is one sample, the impact of the number of transmission repetitions in spectro-temporal combining is significant, even when the probability of interference is as high as 0.4. This is because the positions of the signal samples affected by interference are highly random and spectrum combining can effectively suppress interference, thus maximizing the effect of temporal combining. With a much longer mean interference length of 500 samples, the interference signal becomes bursty,

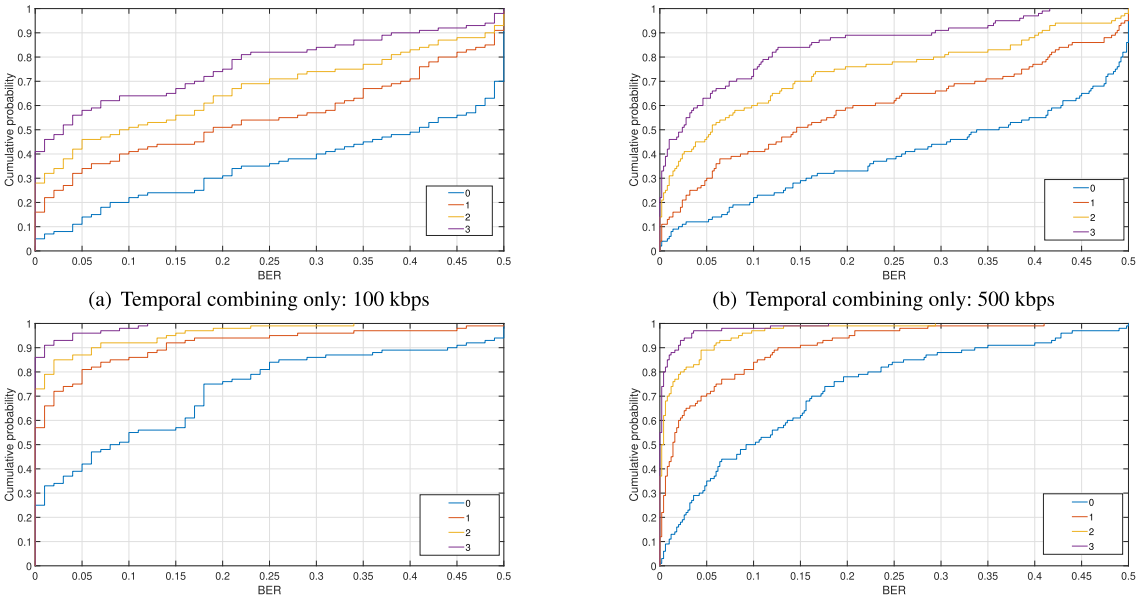

(a) Temporal combining only: 100 kbps

(b) Temporal combining only: 500 kbps

(c) Spectro-temporal combining: 100 kbps

(d) Spectro-temporal combining: 500 kbps

FIGURE 15. Cumulative probability distributions of the per-frame BER for various numbers of transmission repetitions (the carrier frequency is Channel 9).

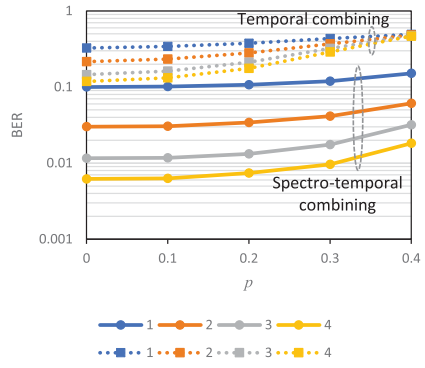

(a) Mean length of interference: 1 sample

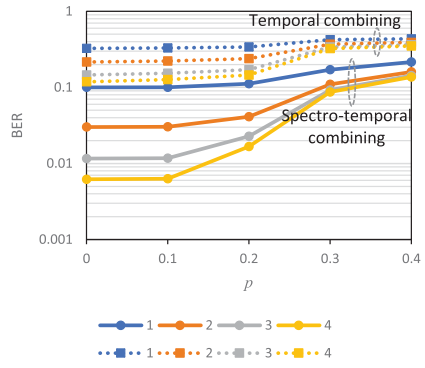

(b) Mean length of interference: 500 samples

FIGURE 16. Impact of interference patterns on BER performance for temporal and spectro-temporal combining schemes with different mean interference lengths and various probabilities of interference.

affecting a wide range of consecutive samples. In this case, the interference suppression effect of spectrum combining becomes limited, and thus, the BER after spectro-temporal combining rapidly increases as the probability of interference increases, as seen in the figure. As also observed in the previous figures, spectro-temporal combining significantly outperforms temporal combining alone under all considered interference patterns.

VI. CONCLUSION

In this paper, we proposed a spectro-temporal combining scheme for bistate backscatter communication using ambient WiFi signals with the frequency shift technique. The proposed scheme allows a receiver to suppress interference in each shifted frequency channel via spectrum combining and to eliminate bit errors due to residual interference via temporal combining at an affordable cost in terms of buffer memory consumption. An experimental study with real WiFi signals demonstrated that the proposed scheme achieves superior BER and throughput performance under diverse communication conditions. The proposed scheme can be combined with or extended to other techniques offering a longer communication range, higher-order modulation, etc., to achieve higher overall performance.

REFERENCES

[1] V. Liu, A. Parks, V. Talla, S. Gollakota, D. Wetherall, and J. R. Smith, "Ambient backscatter: Wireless communication out of thin air," in *Proc. ACM SIGCOMM*, 2013, pp. 39–50.

[2] A. N. Parks, A. Liu, S. Gollakota, and J. R. Smith, "Turbocharging ambient backscatter communication," in *Proc. ACM Conf. SIGCOMM*, Aug. 2014, pp. 619–630.

[3] A. Wang, V. Iyer, V. Talla, J. R. Smith, and S. Gollakota, "FM backscatter: Enabling connected cities and smart fabrics," in *Proc. USENIX NSDI*, 2017, pp. 243–258.

[4] V. Talla, M. Hessar, B. Kellogg, A. Najafi, J. R. Smith, and S. Gollakota, "Lora backscatter: Enabling the vision of ubiquitous connectivity," *Proc. ACM Interact., Mobile, Wearable Ubiquitous Technol.*, vol. 1, no. 3, pp. 1–24, 2017.

[5] M. Zhang, J. Zhao, S. Chen, and W. Gong, "Reliable backscatter with commodity BLE," in *Proc. IEEE Conf. Comput. Commun. (INFOCOM)*, Jul. 2020, pp. 1291–1299.

[6] M. H. Mazaheri, A. Chen, and O. Abari, "Millimeter wave backscatter: Toward batteryless wireless networking at gigabit speeds," in *Proc. ACM HotNets*, 2020, pp. 139–145.

[7] C. Yang, J. Gummeson, and A. Sample, "Riding the airways: Ultra-wideband ambient backscatter via commercial broadcast systems," in *Proc. IEEE Conf. Comput. Commun. (INFOCOM)*, May 2017, pp. 1–9.

[8] T. Kim and W. Lee, "AnyScatter: Eliminating technology dependency in ambient backscatter systems," in *Proc. IEEE Conf. Comput. Commun. (INFOCOM)*, Jul. 2020, pp. 287–296.

[9] W. Gong, L. Yuan, Q. Wang, and J. Zhao, "Multiprotocol backscatter for personal IoT sensors," in *Proc. 16th Int. Conf. Emerg. Netw. Exp. Technol.*, Nov. 2020, pp. 261–273.

[10] B. Kellogg, A. Parks, S. Gollakota, J. R. Smith, and D. Wetherall, "Wi-Fi backscatter: Internet connectivity for RF-powered devices," in *Proc. ACM SIGCOMM*, 2014, pp. 607–618.

[11] P. Zhang, M. Rostami, P. Hu, and D. Ganesan, "Enabling practical backscatter communication for on-body sensors," in *Proc. ACM SIGCOMM Conf.*, Aug. 2016, pp. 370–383.

[12] A. Bletsas, P. N. Alevizos, and G. Vougioukas, "The art of signal processing in backscatter radio for μW (or less) Internet of Things: Intelligent signal processing and backscatter radio enabling batteryless connectivity," *IEEE Signal Process. Mag.*, vol. 35, no. 5, pp. 28–40, Sep. 2018.

[13] G. Vougioukas and A. Bletsas, "Switching frequency techniques for universal ambient backscatter networking," *IEEE J. Sel. Areas Commun.*, vol. 37, no. 3, pp. 464–477, Feb. 2019.

[14] B. Smida and S. Khaledian, "ReflectFX: In-band full-duplex wireless communication by means of reflected power," *IEEE Trans. Commun.*, vol. 65, no. 5, pp. 2207–2219, May 2017.

[15] D. Darsena, G. Gelli, and F. Verde, "Cloud-aided cognitive ambient backscatter wireless sensor networks," *IEEE Access*, vol. 7, pp. 57399–57414, 2019.

[16] X. Liu, Z. Chi, W. Wang, Y. Yao, and T. Zhu, "VMscatter: A versatile MIMO backscatter," in *Proc. USENIX NSDI*, 2020, pp. 895–909.

[17] G. Yang, Y.-C. Liang, R. Zhang, and Y. Pei, "Modulation in the air: Backscatter communication over ambient OFDM carrier," *IEEE Trans. Commun.*, vol. 66, no. 3, pp. 1219–1233, Mar. 2018.

[18] M. A. ElMossallamy, M. Pan, R. Jäntti, K. G. Seddik, G. Y. Li, and Z. Han, "Noncoherent backscatter communications over ambient OFDM signals," *IEEE Trans. Commun.*, vol. 67, no. 5, pp. 3597–3611, May 2019.

[19] D. Darsena, "Noncoherent detection for ambient backscatter communications over OFDM signals," *IEEE Access*, vol. 7, pp. 159415–159425, 2019.

[20] D. Darsena, G. Gelli, and F. Verde, "Modeling and performance analysis of wireless networks with ambient backscatter devices," *IEEE Trans. Commun.*, vol. 65, no. 4, pp. 1797–1814, Jan. 2017.

[21] Y. H. Al-Badarneh, A. Elzanaty, and M.-S. Alouini, "On the performance of spectrum sharing backscatter communication systems," *IEEE Internet Things J.*, early access, Jun. 15, 2021, doi: 10.1109/JIOT.2021.3089500.

[22] D. Bharadia, K. Joshi, M. Kotaru, and S. Katti, "BackFi: High throughput WiFi backscatter," in *Proc. ACM SIGCOMM*, 2017, pp. 283–296.

[23] X. Liu, Z. Chi, W. Wang, Y. Yao, P. Hao, and T. Zhu, "Verification and redesign of OFDM backscatter," in *Proc. USENIX NSDI*, 2021, pp. 939–953.

[24] R. Zhao, F. Zhu, Y. Feng, S. Peng, X. Tian, H. Yu, and X. Wang, "OFDMA-enabled Wi-Fi backscatter," in *Proc. 25th Annu. Int. Conf. Mobile Comput. Netw.*, Aug. 2019.

[25] M. Dunna, M. Meng, P.-H. Wang, C. Zhang, P. Mercier, and D. Bharadia, "SyncScatter: Enabling WiFi like synchronization and range for WiFi backscatter communication," in *Proc. USENIX NSDI*, 2021, pp. 923–937.

[26] A. Abedi, F. Dehbashi, M. H. Mazaheri, O. Abari, and T. Brecht, "WiTAG: Seamless WiFi backscatter communication," in *Proc. ACM SIGCOMM*, 2020, pp. 240–252.

[27] J. Zhao, W. Gong, and J. Liu, "Spatial stream backscatter using commodity WiFi," in *Proc. 16th Annu. Int. Conf. Mobile Syst., Appl., Services*, Jun. 2018, pp. 191–203.

[28] J. Zhao, W. Gong, and J. Liu, "X-Tandem: Towards multi-hop backscatter communication with commodity WiFi," in *Proc. ACM MobiCom*, 2018, pp. 497–511.

[29] X. He, W. Jiang, M. Cheng, X. Zhou, P. Yang, and B. Kurkoski, "GuardRider: Reliable WiFi backscatter using Reed–Solomon codes with QoS guarantee," in *Proc. IEEE/ACM 28th Int. Symp. Qual. Service (IWQoS)*, Jun. 2020, pp. 1–10.

[30] F. Dehbashi, A. Abedi, O. Abari, and T. Brecht, "Verification: Can WiFi backscatter replace RFID?" in *Proc. ACM MobiCom*, 2021, pp. 1–11.

[31] P. Zhang, D. Bharadia, K. Joshi, and S. Katti, "Hitchhike: Practical backscatter using commodity WiFi," in *Proc. ACM SenSys*, 2016, pp. 259–271.

[32] P. Zhang, C. Josephson, D. Bharadia, and S. Katti, "FreeRider: Backscatter communication using commodity radios," in *Proc. ACM CoNEXT*, 2017, pp. 389–401.

[33] H. Hwang, J.-H. Lim, J.-H. Yun, and B. Jeong, "Pattern-based decoding for Wi-Fi backscatter communication of passive sensors," *Sensors*, vol. 19, no. 5, p. 1157, Mar. 2019.

[34] H. Hwang and J.-H. Yun, "Adaptive transmission repetition and combining in bistatic WiFi backscatter communications," *IEEE Access*, vol. 8, pp. 55023–55031, 2020.

[35] T. Kim and W. Lee, "Exploiting residual channel for implicit Wi-Fi backscatter networks," in *Proc. IEEE Conf. Comput. Commun. (INFOCOM)*, Apr. 2018, pp. 1268–1276.

[36] T. Kim and W. Lee, "Channel independent Wi-Fi backscatter networks," in *Proc. IEEE Conf. Comput. Commun. (INFOCOM)*, Apr. 2019, pp. 262–270.

[37] R. Boateng Nti and J.-H. Yun, "Multi-filter decoding in WiFi backscatter communication," *Sensors*, vol. 21, no. 4, p. 1481, Feb. 2021.

[38] Ettus Research. *USRP Networked Series*. Accessed: Aug. 14, 2021. [Online]. Available: http://ettus.com/product-categories/usrp-networked-series/

[39] *GNU Radio*. Accessed: Aug. 14, 2021. [Online]. Available: https://www.gnuradio.org

[40] *Analog Devices, ADG902*. Accessed: Aug. 14, 2021. [Online]. Available: http://www.analog.com/en/design-center/evaluation-hardware-and-software/evaluation-boards-kits/eval-adg902.html

[41] *IGLOO Nano Evaluation Board With AGLN250V2-VQG100*. Accessed: Aug. 14, 2021. [Online]. Available: https://www.microsemi.com/existing-parts/parts/144014

HWANWOONG HWANG received the B.S. and M.S. degrees in electrical and information engineering from Seoul National University of Science and Technology (SeoulTech), Seoul, South Korea, in 2014 and 2016, respectively, where he is currently pursuing the Ph.D. degree in electrical and information engineering. His current research interest includes wireless communications for IoT devices.

RICHARD BOATENG NTI received the B.S. degree in computer engineering from Kwame Nkrumah University of Science and Technology (KNUST), Kumasi, Ghana, in 2014, and the M.S. degree in information and communication engineering from Hanbat National University, Daejeon, South Korea, in 2019. He is currently pursuing the Ph.D. degree in electrical and information engineering with Seoul National University of Science and Technology (SeoulTech), Seoul, South Korea. His current research interest includes wireless communications for IoT devices.

JI-HOON YUN (Member, IEEE) received the B.S. degree in electrical engineering from Seoul National University (SNU), Seoul, South Korea, in 2000, and the M.S. and Ph.D. degrees in electrical engineering and computer science from SNU, in 2002 and 2007, respectively.

He is currently an Associate Professor with the Department of Electrical and Information Engineering, Seoul National University of Science and Technology (SeoulTech), Seoul. Before joining SeoulTech, in 2012, he was with the Department of Computer Software Engineering, Kumoh National Institute of Technology, as an Assistant Professor. He was a Postdoctoral Researcher with the Real-Time Computing Laboratory, The University of Michigan, Ann Arbor, MI, USA, in 2010, and a Senior Engineer with the Telecommunication Systems Division, Samsung Electronics, Suwon, South Korea, from 2007 to 2009. His current research interest includes wireless communications and networking.